Analytical Modeling of the Friction Stir Welding Process Using Different Pin Profiles

Using an analytical approach, it is seen that by increasing the number of edges, the amount of heat generation initially increases from the triangular to square pin profile, then decreases to the hexagon pin profile

BY V. S. GADAKH, A. KUMAR, AND G. J. VIKHE PATIL

ABSTRACT

Friction stir welding (FSW) is considered a combination of extrusion, forging, and stirring of the material where a high strain rate and temperature are generated. Due to the complex nature of heat generation in FSW, the analytical model defines variables and parameters that dominantly affect heat generation, and many of them cannot be fully mathematically explained. This paper proposes an analytical model for heat generation for FSW using different pin profiles such as triangular, square, pentagon, and hexagon. From the obtained results, it is observed that the lowest temperature is generated during welding using the hexagonal pin profile, while the square pin profile has the highest temperature among all pin profiles under the given set of working conditions. Furthermore, the results obtained from numerical modeling show that increasing the tool rotational speed at constant weld speed increases the heat input, whereas the heat input decreases with an increase in the weld speed at constant tool rotational speed. In addition, the paper describes the application of Comsol to thermal modeling in FSW. Different tool pin profiles used for the analysis for heat generation and temperature distribution are also included.

KEYWORDS

• Friction Stir Welding (FSW) • Analytical Modeling • Tool Geometry
• Heat Generation • Aluminum Alloy

Introduction

Traditionally, the heat generation in friction stir welding (FSW) was considered to be due to friction, but practically it is due to friction as well as deformation. Henceforth, it will better to be termed as 'deformation stir welding' rather than FSW (Ref. 1). Heat generation in FSW is a complex transformation process where one part of mechanical energy is delivered to the tool, which is consumed in welding, while another is used for the deformation process and the rest of the energy is transformed into heat (Ref. 2).

In the present work, an analytical model for heat generation using different pin profiles such as triangular (TR), square (SQ), pentagon (PEN), and hexagon (HEX) are developed. As for today, the analytical models developed are for straight cylindrical (SC) (Refs. 3, 4) and taper cylindrical (TC) (Ref. 5) pin profiles.

Khandkar et al. (Ref. 3) introduced a torque-based heat input model for SC pin profile, where the torque/power known from experiments is used in the expression for the heat source. Furthermore, Schmidt et al. (Ref. 4) developed an analytical model for heat generation for SC having a concave shoulder in FSW based on different assumptions in terms of contact condition between the rotating tool surface and workpiece.

The models developed by Schmidt et al. (Ref. 4) and Ulysse (Ref. 5) assume that heat is dominantly generated on the shoulder tip and neglect the heat generated on the probe. Their models show that 80–90% of the mechanical power delivered to the welding tool transforms into heat.

The model developed by Song and Kovačević (Ref. 6) considers all active surfaces in the analysis of heat generation and shows that 60–100% of the mechanical power transforms into heat during FSW. Gadakh and Kumar (Ref. 7) developed an analytical model for heat generation for TC, which is the modification of analytical models developed for SC pin profiles.

Elangovan et al. (Ref. 8) have considered five different pin profiles such as SC, TC, TH (threaded cylindrical), SQ, and TR. They reported that the SQ pin profiled tool exhibited superior tensile properties. Pin profiles with flat faces (SQ and TR) are associated with eccentricity, which produces the pulsating stirring action and causes a reduction in grain size and homogenous redistribution of the second phase

V. S. GADAKH (gadakh_vijay@rediffmail.com) *and A. KUMAR are with the Department of Mechanical Engineering, National Institute of Technology, Warangal, India. GADAKH (PhD research scholar) and G. J. VIKHE PATIL are with the Department of Mechanical Engineering, Amrutvahini College of Engineering, Sangamner, Savitribai Phule University Pune, Pune, India.*

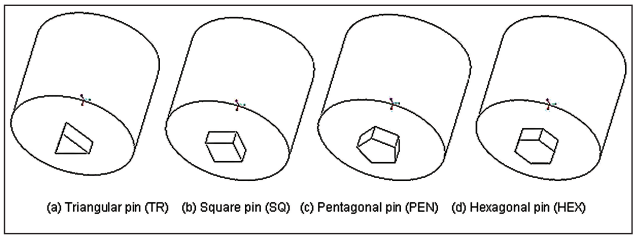

Fig. 1 — Different pin profiles used in FSW.

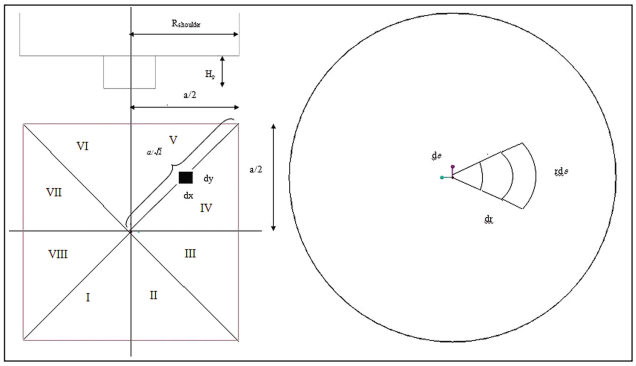

Fig. 3 — Schematic of the surface orientations and infinitesimal segment areas. The top left probe side is Q_2, bottom left square probe is Q_3, and right shoulder surface is also seen.

particles throughout the matrix. Eccentricity of the rotating object is related to the dynamic orbit due to eccentricity.

Khodaverdizadeh et al. (Ref. 9) considered TH and SQ pin profiles. They reported that the SQ pin profile has a finer grain structure, generates higher peak temperature, and higher hardness values. In addition, higher heat generation due to plastic deformation and smaller interfacial contact area with the workpiece leads to lower frictional heat generation relative to the TH pin.

Palanivel et al. (Ref. 10) considered straight (SQ, HEX, octagon (OCT)) and taper (SQ and OCT) pin profiles. They found that the joint fabricated using the straight SQ pin profile yielded highest strength of 273 MPa and tool rotational speed of 950 rev/min.

Fujii et al. (Ref. 11) considered the SC, TH, and TR pin profiles. They reported that in the case of the 1050-H24 aluminum alloy, SC produces a weld with the best mechanical properties. For 6061-T6, the tool shape does not significantly affect the microstructures and mechanical properties of the joints. For 5083-O, at a high rotation speed (1500 rev/min), the TR is the best; at the middle rotation speed (800 rev/min), the TH is the best; while for a low rotation speed (600 rev/min), the tool shape does not significantly affect the microstructures and mechanical properties of the joints.

Vijay and Murugan (Ref. 12) considered three straight (S) and taper (T) SQ, HEX, and OCT pin profiles. They found that for the straight SQ pin profile, it exhibited maximum tensile and joint efficiency, while the taper OCT pin profile exhibited maximum (%) elongation. A defect-free weld is obtained when the taper HEX pin and straight SQ pin tools are used for joining aluminum matrix composites (AMCs).

Padmanaban and Balasubramanian (Ref. 13) considered the SC, TC, TH, TR, and SQ pin profiles. They found that the

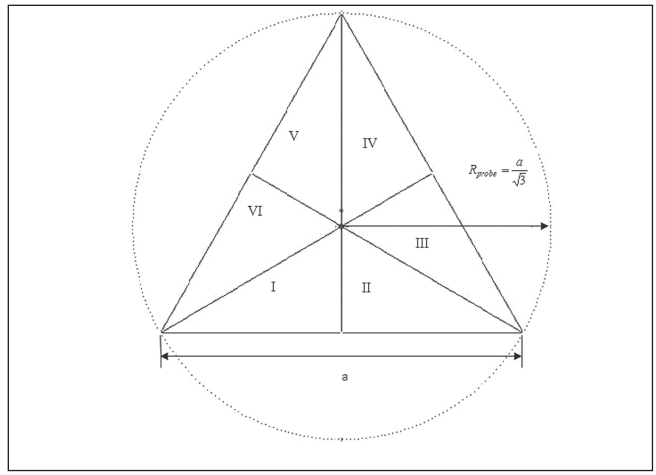

Fig. 2 — Schematic of the triangular probe.

joints fabricated using the TH pin profile yielded a defect-free and fine-grained nugget region, which led to the enhancement of hardness and tensile properties of the welded joints.

Gadakh and Kumar (Ref. 14) developed a process window for the AA 6061-T6 aluminum alloy and obtained a fine-grained structure using the TC pin profile.

Boz and Kurt (Ref. 15) considered five different pin profiles. Four are TH — with 0.85, 1.10, 1.40, and 2.0 mm pitch — and the last SQ with 5 × 5 mm cross section. They have found that the TH with 0.85-mm pitch exhibited maximum elongation (%) and reduction in cross-sectional area (%), and the TH with 1.10-mm pitch exhibited maximum UTS.

Suresha et al. (Ref. 16) have considered TC and SQ profiles for FSW of the AA7075-T6 aluminum alloy. They reported the welded joints produced by the TC tool show better joint efficiency when compared to the SQ tool. Ramanjaneyulu et al. (Ref. 17) studied the influence of different tool pin profiles such as TC; taper (TR, SQ, PEN, and HEX) on heat generation; and microstructure of the AA2014 aluminum alloy. They have reported the rate of heat generation as well as peak temperatures are relatively higher in the case of noncircular pin profiles, increasing with the number of flats (i.e., SQ to HEX) and lowest for TC.

From the reported literature, it is understood that the pin geometry plays a vital role for material flow, temperature history, grain size, and mechanical properties in the FSW process. From these aspects, a question arises why the results are varied for different tool geometries and thereby variations in properties and microstructures. With this consideration, in this paper, an analytical modeling using different tool geometries is considered to estimate the heat generated due to friction between the workpiece and tool surfaces.

Many of the referred literature stated that the failure of friction stir welded joints takes place at the heat-affected zone (HAZ) where the density of the needle-shaped precipitate (β") is less. From the proposed developed models for different tool geometries, one can find the peak temperature at the weld zone so that severe softening in the HAZ (because of the reversion of θ" precipitates during the weld thermal cycle) can be minimized (Ref. 18) by controlling weld process parameters.

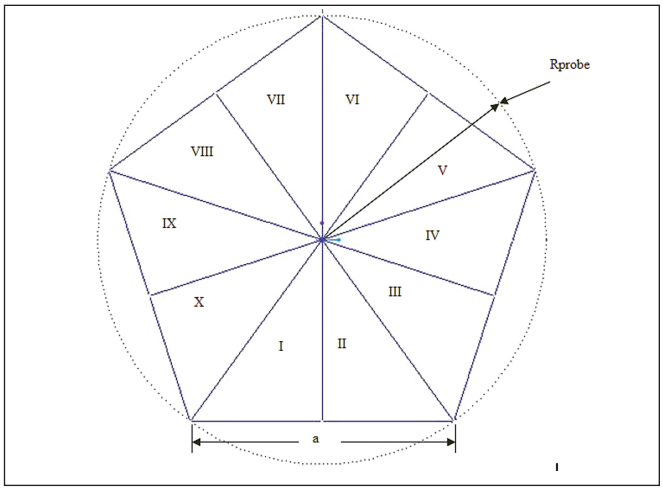

Fig. 4 — Schematic of the pentagonal probe.

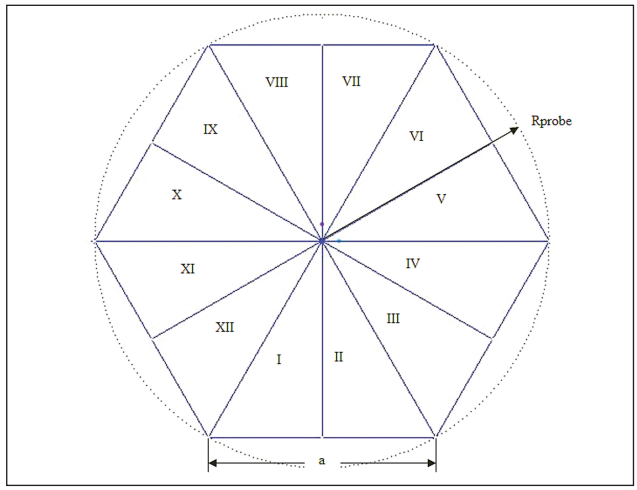

Fig. 5 — Schematic of the hexagonal probe.

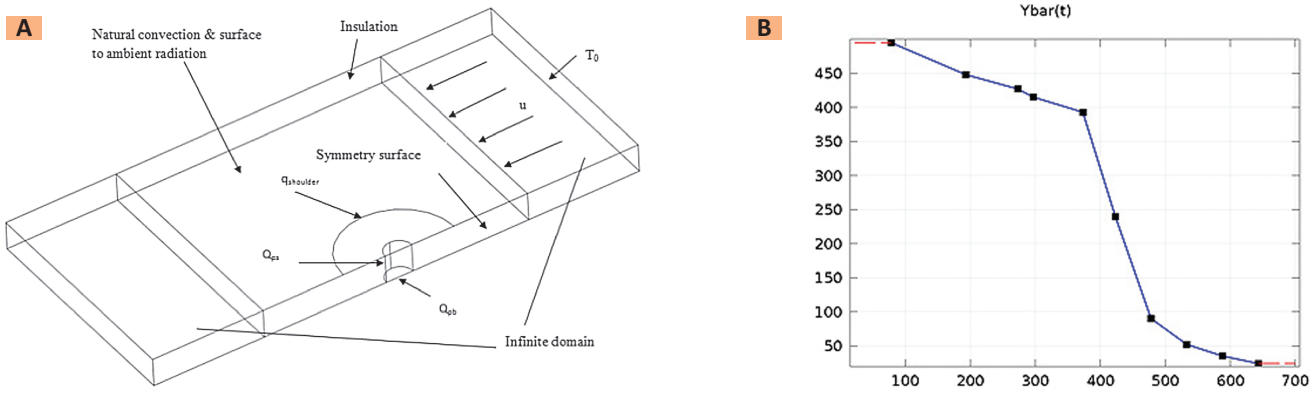

Fig. 6 — A — Model geometry for FSW; B — temperature-dependent 0.2% offset yield strength for AA 2014-T6.

Modeling offers great prospects in the future for reducing experimental efforts in the development of welding parameters, tool and machine designs, clamping systems, and many other areas. Also, with the large effort currently being made in modeling, it is reasonable to expect a significant return on this investment (Ref. 19).

Because of the nature of this approach, the proposed analytical model relies on three major elements — analytic algebra, numerical calculations, and experimental data. The analytic algebra is based on existing research and results but includes some improvements. The algebra is developed for a complete welding tool, involves more dominant parameters in the calculations than in previous models, recognizes more dependencies between parameters, neglects fewer parameters, and has a shorter calculation time (Ref. 19). The numerical method can solve complicated functions that are difficult to be solved by the analytical method. However, a numerical solution is discrete. On the other hand, the analytical method can solve relatively easy functions. Its solution is given by a formula that clearly shows the relationship between independent and dependent variables (Ref. 25).

In this paper, a combined approach of both methods is considered. In the first part, an approximate analytical equation for heat generation is developed for different pin profiles. In the next part, the effect of the different process parameters on the temperature history is shown.

In the present work, analytical modeling of different tool geometries such as TR, SQ, PEN, and HEX (all regular polygons) are developed. The next section is divided into four subsections; the first four sections show proposed analytical models for heat generation for the FSW process on different tool pin geometries, then thermal modeling of different pin geometries using Comsol is presented.

Later, comparison of all tool geometries in terms of total heat generation and peak temperature generated is presented. The FSW process consists of a rotating tool pin penetrating into the two butt joint positioned plates to be joined and transverse motion to the tool. The shoulder surface heats the plate surface due to tool rotation whereas the pin mixes the material from the front of the pin to the back of the pin due to tool rotation and translation.

The following underlying assumptions are made for analytical modeling:

- The analytical estimation based on a general assumption of uniform contact shear stress $\tau_{contact}$ is considered.
- Weld cycle excludes plunging; first, second dwell, and retract cycles.
- Tool inclination angle was not considered.

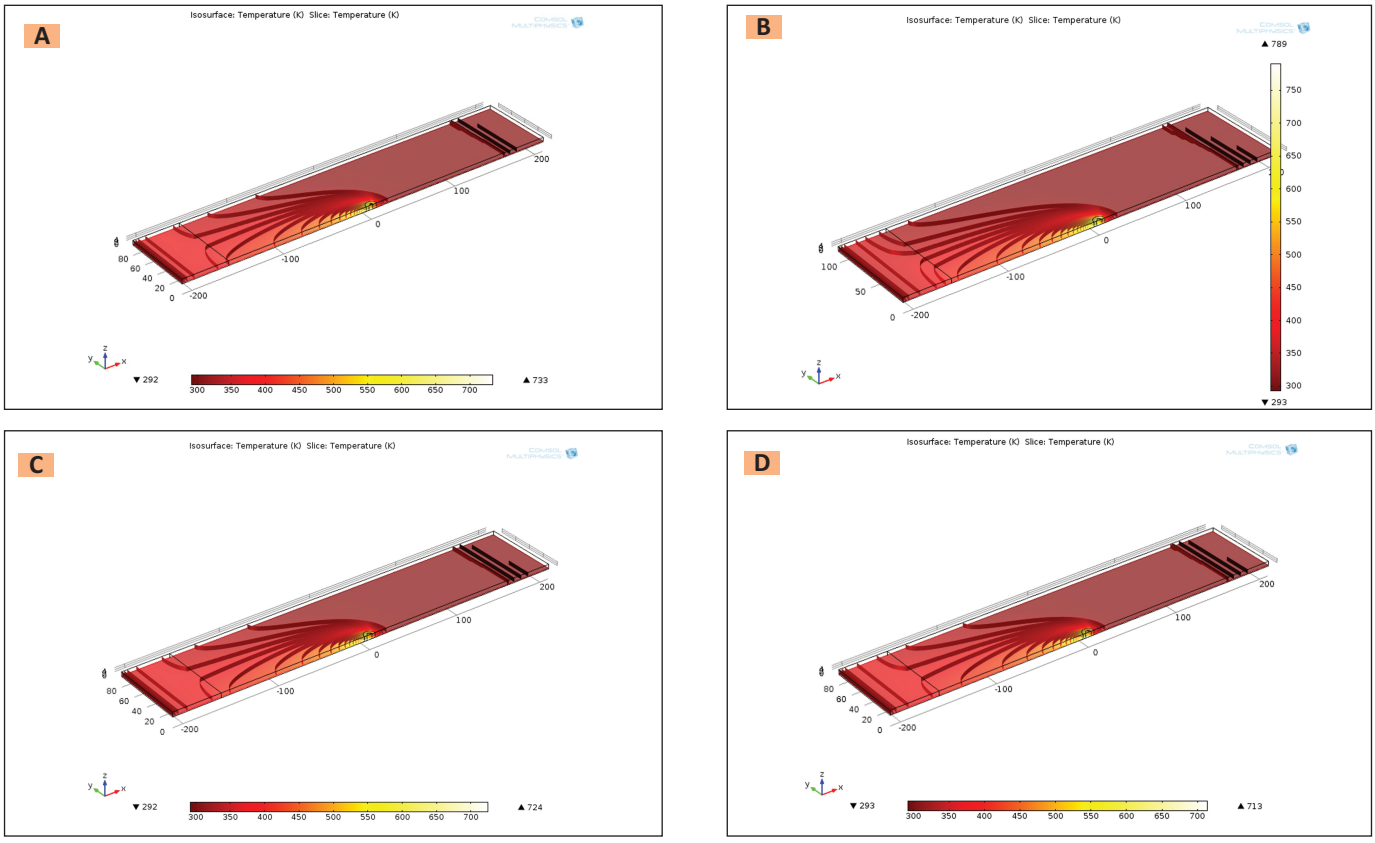

Fig. 7 — Temperature contours for the following: A — TR; B — SQ; C — PEN; and D — HEX pin profile.

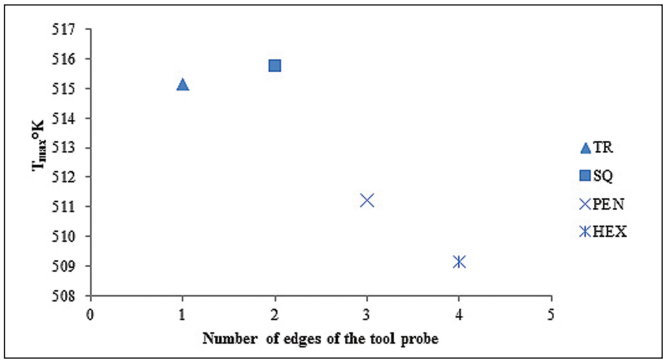

Fig. 8 — Variation in peak temperature with the number of polygon sides.

• No heat flows into the workpiece if the local temperature reaches the material melting temperature.

Due to friction interface conditions, the frictional shear stress $\tau_{friction}$ is considered. The shear stress estimates for a sliding condition is as $\tau_{contact} = \tau_{friction} = \mu p$ (where p = F/Area under shoulder).

Analytical Modeling

Analytical Heat Generation Equation for Triangular Pin Profile

During the FSW process, due to complex geometries of the tool (Fig. 1), the estimation of heat generated at the contact surfaces is quite complex. In the analytical estimation, a simplified tool design with a flat shoulder surface, a vertical SQ prism probe side surface, and a flat probe tip surface is assumed.

The simplified tool design for the TR pin is presented in Fig. 2, where Q_1 is the heat generated under the tool shoulder, Q_2 at the tool SQ probe side, and Q_3 at the tool probe tip, hence the total heat generation, $Q_{total} = Q_1 + Q_2 + Q_3$. To derive the different quantities, the surface under examination is characterized by either being a vertical or horizontal surface. The expressions for each surface orientation are different but are based on the same equation for heat generation:

$$dQ = \omega \cdot dM = \omega \cdot x \cdot dF = \omega \cdot x \cdot \tau_{contact} \cdot dA \qquad (1)$$

Heat generation from shoulder surface is calculated by subtracting the heat generated due to probe tip (Q_3) from the heat generated due to shoulder ($Q_{Shoulder}$) where $a = R_{probe} \cdot \sqrt{3}$ is the side of the TR pin profile. Thus, heat generated due to the shoulder is given by Frigaard et al. (Refs. 20, 21) as

$$Q_{shoulder} = \frac{2}{3} \cdot \pi \cdot \omega \cdot \tau_{contact} \cdot R^3_{shoulder} \qquad (2)$$

Therefore, Q_1 is calculated as $Q_{shoulder} - Q_3$, i.e., Equations 2–5

$$Q_1 = \frac{2}{3} \cdot \pi \cdot \omega \cdot \tau_{contact} \cdot R^3_{shoulder} - \frac{2 \cdot \pi \cdot \omega \cdot \tau_{contact} \cdot a^3}{9\sqrt{3}} \qquad (3)$$

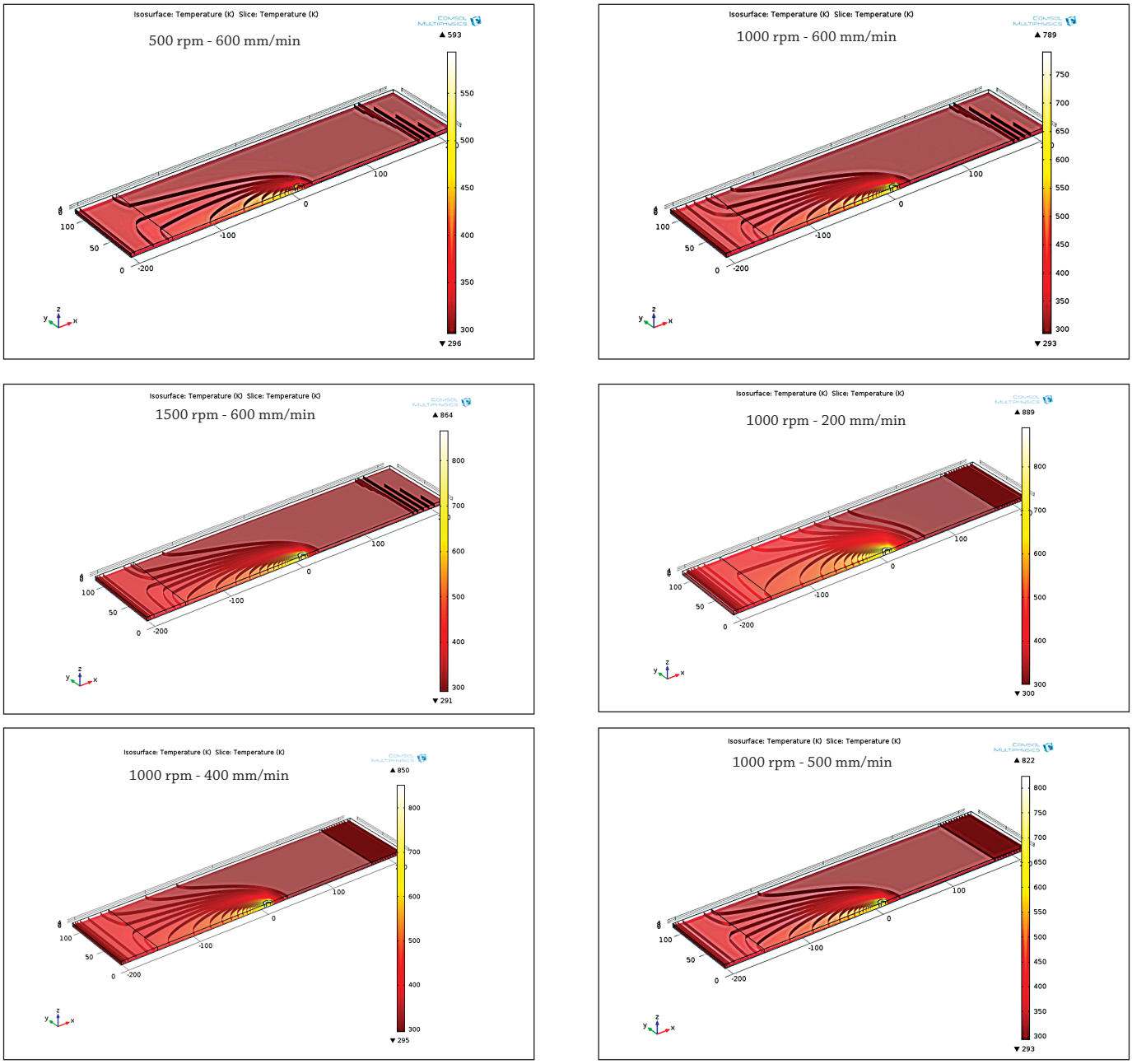

Fig. 9 — Numerical modeling of the SQ pin profile under different process conditions.

Heat generation from the probe surface is

$$Q_2 = \int_{R_{probe}=0}^{R_{probe}=a} \int_{H=0}^{H=H_{probe}} \omega \cdot \tau_{contact} \cdot R_{probe} \cdot dx \cdot dy \qquad (4)$$

The multiplying factor 3 denotes the three sides of the TR probe. Heat generation from the tip surface by using a polar coordinate,

$$Q_3 = \int_{\theta=0}^{\theta=\frac{\pi}{3}} \int_{R_{probe}=0}^{R_{probe}=\frac{a}{\sqrt{3}}} \omega \cdot \tau_{contact} \cdot R^2{}_{probe} \cdot d\theta \cdot dr \quad (5)$$

The multiplying factor 6 denotes the six different regions that form the whole TR surface. From Equations 3, 4, and 5, Q_{Total} can be calculated as $Q_{Total} = Q_1 + Q_2 + Q_3$

$$Q_{Total} = \frac{2}{3}\cdot\pi\cdot\omega\cdot\tau_{contact}\cdot R^3_{shoulder} - \frac{2\cdot\pi\cdot\omega\cdot\tau_{contact}\cdot a^3}{9\sqrt{3}}$$
$$+\frac{1}{2}\cdot\omega\cdot\tau_{contact}\cdot a^2\cdot H_{probe} + \frac{2\cdot\pi\cdot\omega\cdot\tau_{contact}\cdot a^3}{9\sqrt{3}}$$
$$Q_{Total} = \frac{2}{3}\cdot\pi\cdot\omega\cdot\tau_{contact}\cdot R^3_{shoulder} + \frac{1}{2}\cdot\omega\cdot\tau_{contact}\cdot a^2\cdot H_{probe}$$
$$Q_{Total} = \frac{2}{3}\cdot\pi\cdot\omega\cdot\tau_{contact}\cdot\left(R^3_{shoulder} + \frac{3}{4\pi}\cdot a^2\cdot H_{probe}\right)$$

or

$$Q_{Total} = \frac{2}{3}\cdot\pi\cdot\omega\cdot\tau_{contact}\cdot\left(R^3_{shoulder} + \frac{9}{4\pi}\cdot R^2_{probe}\cdot H_{probe}\right) \quad (6)$$

The energy per unit length of the weld can be calculated as dividing Equation 6 by weld speed (υ) as

$$Q_{Energy/length} = \frac{2}{3}\cdot\frac{\omega\cdot\mu\cdot F}{\upsilon\cdot R^2_{shoulder}}\cdot\left(R^3_{shoulder} + \frac{3}{4\pi}\cdot a^2\cdot H_{probe}\right)$$

or

$$Q_{Energy/length} = \frac{2}{3}\cdot\frac{\omega\cdot\mu\cdot F}{\upsilon\cdot R^2_{shoulder}}\cdot\left(R^3_{shoulder} + \frac{9}{4\pi}\cdot R^2_{probe}\cdot H_{probe}\right) \quad (7)$$

Where $\tau_{contact} = \tau_{friction} = \mu p = \mu\sigma$, pressure equals the force divided by the projected area.

Analytical Heat Generation Equation for Square Pin Profile

The heat generation from the shoulder surface is calculated by subtracting the heat generated due to probe tip (Q_3) from the heat generated due to the shoulder ($Q_{Shoulder}$) where $a = R_{probe}\cdot\sqrt{2}$ is the side of the SQ.

Top Left Probe Side (Q_2), Bottom Left Square Probe (Q_3), and Right Shoulder Surface

Similarly, the heat generation from the tip surface (Q_3) is given by the general expression (1) from Fig. 3 (bottom left), an infinitesimal segment having the width *dx* and height *dy* by considering only 1/8th part, which is integrated and converted from rectangular to polar coordinates with the limits given in the below expression as follows:

$$Q_3 = \int_{\theta=0}^{\theta=\frac{\pi}{4}}\int_{R_{probe}=0}^{R_{probe}=\frac{a}{\sqrt{2}}} \omega\cdot\tau_{contact}\cdot R_{probe}\cdot R_{probe}\cdot d\theta\cdot dr \quad (8)$$

The multiplication term 8 denotes the eight different regions that form a SQ surface. Therefore, Q_1 is calculated as $Q_{shoulder} - Q_3$, i.e., Equations 2–8

$$Q_1 = \frac{2}{3}\cdot\pi\cdot\omega\cdot\tau_{contact}\cdot R^3_{shoulder} - \frac{\pi\cdot\omega\cdot\tau_{contact}\cdot a^3}{3\sqrt{2}} \quad (9)$$

With the heat generation from the probe surface, considering rectangular coordinates, we get

$$Q_2 = \int_{R_{probe}=0}^{R_{probe}=a}\int_{H=0}^{H=H_{probe}} \omega\cdot\tau_{contact}\cdot R_{probe}\cdot dx\cdot dy$$
$$= \omega\cdot\tau_{contact}\cdot\frac{a^2}{4}\cdot H_{probe} \quad (10)$$

The multiplication term 4 denotes the four sides of the SQ probe. From Equations 8–10, Q_{Total} can be calculated as $Q_{Total} = Q_1 + Q_2 + Q_3$

$$Q_{Total} = \frac{2}{3}\cdot\pi\cdot\omega\cdot\tau_{contact}\cdot R^3_{shoulder} - \frac{\pi\cdot\omega\cdot\tau_{contact}\cdot a^3}{3\sqrt{2}}$$
$$+\omega\cdot\tau_{contact}\cdot a^2\cdot H_{probe} + \frac{\pi\cdot\omega\cdot\tau_{contact}\cdot a^3}{3\sqrt{2}}$$
$$Q_{Total} = \frac{2}{3}\cdot\pi\cdot\omega\cdot\tau_{contact}\cdot R^3_{shoulder} + \omega\cdot\tau_{contact}\cdot a^2\cdot H_{probe}$$
$$Q_{Total} = \frac{2}{3}\cdot\pi\cdot\omega\cdot\tau_{contact}\cdot\left(R^3_{shoulder} + \frac{3}{2\pi}\cdot a^2\cdot H_{probe}\right)$$

or

$$Q_{Total} = \frac{2}{3}\cdot\pi\cdot\omega\cdot\tau_{contact}\cdot\left(R^3_{shoulder} + \frac{3}{\pi}\cdot R^2_{probe}\cdot H_{probe}\right) \quad (11)$$

The energy per unit length of the weld can be calculated by dividing Equation 11 by the weld speed (υ) as

$$Q_{Energy/length} = \frac{2}{3}\cdot\frac{\omega\cdot\mu\cdot F}{\upsilon\cdot R^2_{shoulder}}\cdot\left(R^3_{shoulder} + \frac{3}{2\pi}\cdot a^2\cdot H_{probe}\right)$$

or

$$Q_{Energy/length} = \frac{2}{3}\cdot\frac{\omega\cdot\mu\cdot F}{\upsilon\cdot R^2_{shoulder}}\cdot\left(R^3_{shoulder} + \frac{3}{\pi}\cdot R^2_{probe}\cdot H_{probe}\right) \quad (12)$$

Analytical Heat Generation Equation for Pentagonal Pin Profile

The heat generation from the shoulder surface is calculated by subtracting the heat generated due to the probe tip (Q_3) from the heat generated due to shoulder ($Q_{Shoulder}$). $a = R_{probe}/0.8506$ is the side of the PEN pin profile. The simplified tool design for the PEN pin is presented in Fig. 4.

Therefore, Q_1 is calculated as $Q_{shoulder} - Q_3$, i.e., Equations 2–15

$$Q_1 = \frac{2}{3}\cdot\pi\cdot\omega\cdot\tau_{contact}\cdot R^3{}_{shoulder} - \frac{2\times 0.6155\cdot\pi\cdot\omega\cdot\tau_{contact}\cdot a^3}{3} \quad (13)$$

The heat generation from the probe surface represents

$$Q_2 = \int_{R_{probe}=0}^{R_{probe}=a}\int_{H=0}^{H=H_{probe}} R_{probe}\cdot\omega\cdot\tau_{contact}\cdot dx\cdot dy$$

$$= 0.36176\cdot\omega\cdot\tau_{contact}\cdot a^2\cdot H_{probe}$$

$$Q_2 = 5\times 0.36176\times a\cdot\omega\cdot\tau_{contact}\cdot a^2\cdot H_{probe}$$

$$= 1.8088\cdot\omega\cdot\tau_{contact}\cdot a^2\cdot H_{probe} \quad (14)$$

The factor 5 denotes the five sides of the PEN probe. Heat generation from the tip surface is

$$Q_3 = \int_{\theta=0}^{\theta=\frac{\pi}{5}}\int_{R_{probe}=0}^{R_{probe}=0.8506a} \omega\cdot\tau_{contact}\cdot R_{probe}\cdot R_{probe}\cdot d\theta\cdot dr \quad (15)$$

The factor 10 denotes the ten different regions that form a PEN surface. From Equations 13–15, Q_{Total} can be calculated as $Q_{Total} = Q_1 + Q_2 + Q_3$

$$Q_{Total} = \frac{2}{3}\cdot\pi\cdot\omega\cdot\tau_{contact}\cdot R^3{}_{shoulder} - \frac{2\times 0.6155\cdot\pi\cdot\omega\cdot\tau_{contact}\cdot a^3}{3}$$

$$+1.8088\cdot\omega\cdot\tau_{contact}\cdot a^2\cdot H_{probe} + \frac{2\times 0.6155\cdot\pi\cdot\omega\cdot\tau_{contact}\cdot a^3}{3}$$

$$Q_{Total} = \frac{2}{3}\cdot\pi\cdot\omega\cdot\tau_{contact}\cdot R^3{}_{shoulder} + 1.8088\cdot\omega\cdot\tau_{contact}\cdot a^2\cdot H_{probe}$$

$$Q_{Total} = \frac{2}{3}\cdot\pi\cdot\omega\cdot\tau_{contact}\cdot\left(R^3{}_{shoulder} + \frac{3}{2\pi}1.8088\cdot a^2\cdot H_{probe}\right)$$

or

$$Q_{Total} = \frac{2}{3}\cdot\pi\cdot\omega\cdot\tau_{contact}\cdot\left(R^3{}_{shoulder} + \frac{3.75}{\pi}\cdot R^2{}_{probe}\cdot H_{probe}\right) \quad (16)$$

The energy per unit length of the weld can be calculated as dividing Equation 16 by weld speed (υ) as

$$Q_{Energy/length} = \frac{2}{3}\cdot\frac{\omega\cdot\mu\cdot F}{\upsilon\cdot R^2{}_{shoulder}}\cdot\left(R^3{}_{shoulder} + \frac{3}{2\pi}1.8088\cdot a^2\cdot H_{probe}\right)$$

or

$$Q_{Energy/length} = \frac{2}{3}\cdot\frac{\omega\cdot\mu\cdot F}{\upsilon\cdot R^2{}_{shoulder}}\cdot\left(R^3{}_{shoulder} + \frac{3.75}{\pi}\cdot R^2{}_{probe}\cdot H_{probe}\right) \quad (17)$$

Analytical Heat Generation Equation for Hexagonal Pin Profile

Figure 5 shows the simplified tool design for the HEX pin profile. The heat generation from the shoulder surface is calculated by subtracting the heat generated due to the probe tip (Q_3) from the heat generated due to the shoulder ($Q_{Shoulder}$). $a = R_{probe}$ is the side of the HEX pin.

Therefore, Q_1 is calculated as $Q_{shoulder} - Q_3$, i.e., Equations 2–20

$$Q_1 = \frac{2}{3}\cdot\pi\cdot\omega\cdot\tau_{contact}\cdot R^3{}_{shoulder} - \frac{2\cdot\pi\cdot\omega\cdot\tau_{contact}\cdot a^3}{3} \quad (18)$$

The heat generation from the probe surface is

$$Q_2 = \int_{R_{probe}=0}^{R_{probe}=a}\int_{H=0}^{H=H_{probe}} R_{probe}\cdot\omega\cdot\tau_{contact}\cdot dx\cdot dy = \omega\cdot\tau_{contact}\cdot\frac{a^2}{2}\cdot H_{probe}$$

$$Q_2 = 6\cdot\omega\cdot\tau_{contact}\cdot\frac{a^2}{2}\cdot H_{probe} = 3\cdot\omega\cdot\tau_{contact}\cdot a^2\cdot H_{probe} \quad (19)$$

The factor 6 denotes the six sides of the HEX probe. Heat generation from tip surface is as follows:

$$Q_3 = \int_{\theta=0}^{\theta=\frac{\pi}{6}}\int_{R_{probe}=0}^{R_{probe}=a} \omega\cdot\tau_{contact}\cdot R_{probe}\cdot R_{probe}\cdot d\theta\cdot dr$$

$$Q_3 = \frac{\pi\cdot\omega\cdot\tau_{contact}\cdot a^3}{18} = 12\times\frac{\pi\cdot\omega\cdot\tau_{contact}\cdot a^3}{18}$$

$$Q_3 = \frac{2\cdot\pi\cdot\omega\cdot\tau_{contact}\cdot a^3}{3} \quad (20)$$

The factor 12 denotes the twelve different regions that form a HEX surface. From Equations 18–20, Q_{Total} can be calculated as $Q_{Total} = Q_1 + Q_2 + Q_3$.

$$Q_{Total} = \frac{2}{3}\cdot\pi\cdot\omega\cdot\tau_{contact}\cdot R^3{}_{shoulder} - \frac{2\cdot\pi\cdot\omega\cdot\tau_{contact}\cdot a^3}{3}$$

$$+3\cdot\omega\cdot\tau_{contact}\cdot a^2\cdot H_{probe} + \frac{2\cdot\pi\cdot\omega\cdot\tau_{contact}\cdot a^3}{3}$$

$$Q_{Total} = \frac{2}{3}\cdot\pi\cdot\omega\cdot\tau_{contact}\cdot R^3{}_{shoulder} + 3\cdot\omega\cdot\tau_{contact}\cdot a^2\cdot H_{probe}$$

$$Q_{Total} = \frac{2}{3}\cdot\pi\cdot\omega\cdot\tau_{contact}\cdot\left(R^3{}_{shoulder} + \frac{9}{2\pi}\cdot a^2\cdot H_{probe}\right)$$

or

$$Q_{Total} = \frac{2}{3}\cdot\pi\cdot\omega\cdot\tau_{contact}\cdot\left(R^3{}_{shoulder} + \frac{9}{2\pi}\cdot R^2{}_{probe}\cdot H_{probe}\right) \quad (21)$$

The energy per unit length of the weld can be calculated as dividing Equation 21 by the weld speed (υ) as

$$Q_{Energy/length} = \frac{2}{3} \cdot \frac{\omega \cdot \mu \cdot F}{\upsilon \cdot R^2_{shoulder}} \cdot \left(R^3_{shoulder} + \frac{9}{2\pi} \cdot a^2 \cdot H_{probe} \right)$$

or

$$Q_{Energy/length} = \frac{2}{3} \cdot \frac{\omega \cdot \mu \cdot F}{\upsilon \cdot R^2_{shoulder}} \cdot \left(R^3_{shoulder} + \frac{9}{2\pi} \cdot R^2_{probe} \cdot H_{probe} \right) \quad (22)$$

Thermal Modeling

The thermal-pseudo-mechanical model (TPM) for different pin profiles such as TR, SQ, PEN, and HEX is developed using the heat transfer module in Comsol 4.4.

The model geometry is symmetric around the weld; hence, only one aluminum plate is modeled. The aluminum Alloy AA 2014-T6 plate dimensions are 320 × 80 × 5 mm, surrounded by two infinite domains in the x direction. The shoulder and pin diameters were kept constant for all tools at 12 and 6 mm. For different geometries, the tool rotational speed at 1000 rev/min and weld speed at 600 mm/min were kept constant. The values of axial force were 9.09 kN for TR, 8.97 kN for SQ, 6.98 kN for PEN, and 6 kN for the HEX pin profile (Ref. 17).

The temperature distribution is obtained by solving the energy equation, expressed here as the conductive-convective, steady-state equation (Ref. 5).

$$\rho C_p u \cdot \nabla\theta = \nabla \cdot (k \nabla\theta) + \dot{Q} \quad (23)$$

where ρ is density, C_p the specific heat, u the velocity vector, k thermal conductivity, θ the temperature, and $\dot{Q}$ is the internal heat generation rate.

Boundary Conditions and Initial Condition

The model geometry is symmetric around the weld. Hence, only one aluminum plate is sufficient to model.

Figure 6A shows the resulting model geometry. The temperature-dependent yield stress is shown in Fig. 6B. The heat flux boundary condition for the workpiece at the tool shoulder/workpiece interface is $Q_{shoulder}$. Similarly, the heat flux boundary condition at the tool pin/workpiece interface and tool shoulder/workpiece interface is Q_2 and Q_3, respectively. $Q_{shoulder}$, Q_2, and Q_3 can be calculated by respective equations for different pin profiles.

The inbuilt material properties for the AA 2014-T6 aluminum alloy were considered, and for AISI H13 tool steel, are as follows: thermal conductivity – 36 [W/(m·K)], density – 7833 [kg/m^3], and heat capacity at constant pressure – 460 [J/(kg·K)]. Mesh size for the model is as follows: maximum element size – 8.4 mm, minimum element size – 0.084, and maximum element growth rate – 1.3.

The element type and amount used in this study are as follows: prism elements – 142, hexahedral elements – 1352, triangular elements – 142, quadrilateral elements – 1698, and edge elements – 374.

Convection Boundary Conditions

The upper and lower surfaces of the aluminum plates lose heat due to natural convection and surface to ambient radiation. The h_{up} and h_{down} are heat transfer coefficients for natural convection. In the present study, it is considered as 12.25 and 6.25 W/m^{2}K, respectively.

Figure 7A–D shows temperature isotherms for different pin profiles. The peak temperature among different pin profile is monotonous. The highest peak temperature is for the SQ pin profile (789 K) and lowest for HEX pin profile (713 K), whereas the trend is increases from TR (733 K) to SQ (789 K), then decreasing from PEN pin profile (724 K) to HEX pin profile (713 K). Furthermore, the peak temperature in case of conical tool geometry from TR-HEX pin profiles was also monotonous (Ref. 17). It was reported that the HEX pin profile has the highest peak temperature and lowest for SQ pin profile. The peak temperature trend is decreases from HEX-TR-PEN-SQ pin profile.

Results and Discussion

The effective energy per weld length (Q_{Eff}) (Ref. 22) is defined as the energy per weld length multiplied by the transfer efficiency (β, ratio of the pin length H_{Probe} to the workpiece thickness, t) and given as follows:

$$Q_{Eff} = \frac{h}{t} \cdot Q_{Energy/Length} = \beta \cdot Q_{Energy/Length} \quad (24)$$

For validation of the proposed model, the empirical relationship developed by Hamilton et al. (Ref. 22) between the temperature ratio and effective energy level is considered. The empirical formula is given by

$$\frac{T_{max}}{T_s} = 1.56 \times 10^{-4} \times Q_{Eff} + 0.54 \quad (25)$$

It is agreed that the above expression will change for different work material and one has to find this expression by trial experiments.

Table 1 — Summary of Different Pin Profiles Showing $Q_{Energy/Length}$, and T_{max}

Pin Profile	$Q_{(Energy/length)}$ J/mm	$Q_{(Energy/length)}$, Eff.	T_{max}/T_s	T_{max} (K) (Analytical)	T_{max} (K) (Numerical)	T_{max} (K) (Ref. 17)
TR	173.67	163.25	0.565	515	733	614
SQ	178.40	167.70	0.566	516	789	619
PEN	144.29	135.63	0.561	511	724	623
HEX	128.73	121.01	0.559	509	713	637

The analytical model gives precise results only if experimentally estimated parameters are involved in the model. Furthermore, verification of the analytical model can be done by comparing the results from the analytical model with experimentally estimated results (Ref. 2). The friction coefficient (μ) varies with temperature. However, in the present model for demonstration purposes, it is considered as 0.4.

The summary of all pin profiles shown in Table 1, under the following process parameters, are as follows: tool rotational speed – 1000 rev/min, weld speed – 10 mm/s, μ – 0.4, $R_{shoulder}$ – 6 mm, R_{probe} – 3 mm, and H_{probe} – 4.7 mm. The AA2014-T6 thickness is 5 mm, solidus temperature – 780 K, liquidus temperature – 911 K, F - 9.09 kN for TR, 8.97 kN for SQ, 6.98 kN for PEN, and 6 kN for the HEX pin profile.

The expression for heat generation in FSW is given below in a generalized form where the value of multiplying factor '*X*' is 3 (Ref. 4). The value of '*X*' for different pin profiles is shown in Table 2. From Table 2, it is seen that by increasing the sides of polygon, the value of '*X*' goes on increasing and finally it stops at value 3.

$$Q_{Total} = \frac{2}{3} \cdot \pi \cdot \omega \cdot \mu \cdot \tau_{contact} \cdot \left(R^3_{shoulder} + X \cdot R^2_{probe} \cdot H_{probe} \right) \quad (26)$$

From Table 1, it is seen that heat generation of given pin profiles in ascending order of the edges initially increases from the TR to SQ pin profile, then decreases to the HEX pin profile. From Table 2, it is seen that an increase in the number of edges leads to an increase in the pulsating stirring action, but a decrease in the heat and temperature profile of the weld zone under the given set of process conditions.

From Fig. 8, it can be seen that increasing the number of edges, the peak temperature initially increases from the TR to SQ pin profile then decreases to the HEX pin profile. Furthermore, an increase in number of edges that finally forms a circle means the heat generation is lowest for the SC pin profile, beyond which no temperatures rise.

Figure 9 and Table 3 shows the modeling heat generation for the SQ pin profile with peak temperature and its comparison with the developed analytical model.

The variation in analytical and numerical modeling using Comsol is attributed due to the following two reasons: First, in numerical modeling, material properties such as thermal conductivity, heat capacity, and density of both the workpiece and tool material were considered (i.e., material specific), whereas in analytical modeling only process parameters were considered (i.e., nonmaterial specific). Second, the friction coefficient was assumed and Equation 25 adapted from Ref. 22, when the analytical method is used.

From Table 3, it is seen that under constant weld speed and increasing tool rotational speed, heat input increases and hence peak temperature increases. This agrees well with literature (Ref. 8) where it was reported that varying tool rotational speed could raise strain rate, and thereby influence the recrystallization process. Similarly, under constant tool rotational speed and increasing weld speed, heat input decreases and hence peak temperature decreases. This agrees well with literature (Ref. 26), where it was reported that at lower weld speed, overaging takes place in the weld region due to high frictional heat generation and at higher weld speed underaging take place due to low frictional heat generation.

Moreover, process maps for different work material (Ref. 23) gives a clear understanding regarding temperature, strain rate, plastic deformation, and behavior, which will be helpful to optimize the FSW tool geometry and process parameters to get defect-free welds.

Recently, a similar approach was developed by Backer et al. (Ref. 24) where they used a temperature controller that modifies the spindle speed to maintain a constant welding temperature except predicting the mechanical properties. The correlation of temperature data by considering the deformation with strain rate, Zener-Holloman parameter, and grain size will remain as a future work.

Conclusions

Understanding the process of heat generation and estimating the amount of heat generated during FSW are complex and challenging tasks that require a multidisciplinary approach.

In this study, an analytical model for heat generation in FSW of aluminum alloys using different pin profiles such as TR, SQ, PEN, and HEX are developed. Using an analytical approach, it is seen that by increasing the number of edges, the amount of heat generation initially increases from the TR to SQ pin profile, then decreases to the HEX pin profile. Furthermore, numerical modeling shows that increasing the

Table 2 — Different Pin Profiles with Multiplying Factor 'X'

Pin Profile	Multiplying Factor (X)
TR	0.72
SQ	0.95
PEN	1.19
HEX	1.43
SC	3

Table 3 — Numerical Modeling of SQ Pin Profile under Different Process Conditions

Sr. No.	Condition	$Q_{(Energy/length)}$, J/mm	$Q_{(Energy/length)}$, Eff.	T_{max} (K) (Analytical)	T_{max} (K) (Numerical)
A	500–600	89.20	83.85	504	593
B	1000–600	178.40	167.70	516	789
C	1500–600	267.60	251.54	528	864
D	1000–200	535.20	503.09	563	889
E	1000–400	267.60	251.54	528	850
F	1000–500	214.08	201.23	521	822

Note: 500–600 = 500 rev/min (tool rotational speed) – 600 mm/min (weld speed) all at 8.97 kN (vertical force) condition.

tool rotational speed under constant weld speed, heat input increases, and increasing the weld speed under constant tool rotational speed, heat input decreases. With the proposed analytical approach, one can directly seek the peak temperature for respective tool geometry under given process conditions, which will be helpful for predicting the mechanical properties by correlating with the precipitate phase distribution for that aluminium alloy.

The proposed analytical model gives precise results only if experimentally estimated parameters are involved in the model. In addition to this, a process map for the defect-free joints can be obtained using a material flow pattern.

Acknowledgments

The authors would like to acknowledge the valuable advice and expertise provided by Dr. G. Madhusudhan Reddy of Defence Metallurgical Research Laboratory (DMRL), Hyderabad. In addition, the authors would like to thank the authorities of the National Institute of Technology (NIT), Warangal, India. One of the authors (V. S. Gadakh) gratefully acknowledges the support of the BCUD, Savitribai Phule University Pune, Pune Grant # 13ENG000074. Also, the authors would like to express their gratitude to the anonymous referees for their valuable comments and suggestions that contributed significantly to improving the quality of this paper.

Nomenclature

Q_1 = heat generation from the shoulder surface
Q_2 = heat generation from the probe surface
Q_3 = heat generation from the tip surface
μ = friction coefficient
ω = tool angular rotation speed/rad s^{-1}
υ = tool speed of ωr/ms^{-1}
σ = contact pressure/Pa
$\tau_{Contact}$ = contact shear stress/Pa
R_{Probe} = tool probe radius/mm
$R_{Shoulder}$ = tool shoulder radius/mm
Q_{Total} = total heat generation/W
H_{Probe} = tool probe height/mm
F = axial force/N

References

1. Reddy, G. M. 2014. Friction stir welding. Keynote lecture at a national workshop on friction stir welding, NDT, and optimization, Jan. 9–11 at NIT, Warangal, A. P. India.

2. Mijajlović, M., and Milčić, D. Analytical model for estimating the amount of heat generated during friction stir welding: Application on plates made of aluminium alloy 2024-T351, p. 247–274. doi. 10.5772/53563.

3. Khandkar, M. Z. H., Khan, J. A., and Reynolds, A. P. 2003. Prediction to temperature distribution and thermal history during friction stir welding: Input torque based model. *Sci. Technol. Weld. Join.* 8: 165–174.

4. Schmidt, H., Hattel, J., and Wert, J. 2004. An analytical model for the heat generation in friction stir welding. *Modelling Simul. Mater. Sci. Eng.* 12: 143–157.

5. Ulysse, P. 2002. Three-dimensional modeling of the friction stir welding process. *Int. J. Mach. Tools. Manuf.* 42: 1549–1557.

6. Song, M., and Kovačević, R. 2003. Thermal modeling of friction stir welding in a moving coordinate system and its validation. *Int. J. Mach. Tools. Manuf.* 43(6): 605–615.

7. Gadakh, V. S., and Kumar, A. 2013. Heat generation model for taper cylindrical pin profile in friction stir welding. *J. Mater. Res. Technol.* 2(4): 370–375.

8. Elangovan, K., Balasubramanian, V., and Valliappan, M. 2008. Effect of tool pin profile and tool rotational speed on mechanical properties of friction stir welded AA6061 aluminium alloy. *Mater. Manuf.* 23(3): 251–260.

9. Khodaverdizadeh, H., Heidarzadeh, A., and Saeid, T. 2013. Effect of tool pin profile on microstructure and mechanical properties of friction stir welded pure copper joints. *Mater. Des.* 45: 265–270.

10. Palanivel, R., Mathews, P. K., Murugan, N., and Dinaharan, I. 2012. Effect of tool rotational speed and pin profile on microstructure and tensile strength of dissimilar friction stir welded AA5083-H111 and AA6351-T6 aluminium alloys. *Mater. Des.* 40: 7–16.

11. Fujii, H., Cui, L., Maeda, M., and Nogi, K. 2006. Effect of tool shape on mechanical properties and microstructure of friction stir welded aluminium alloys. *Mater. Sci. Eng. A.* 419: 25–31.

12. Vijay, S. J., and Murugan, N. 2010. Influence of tool pin profile on the metallurgical and mechanical properties of friction stir welded Al–10 wt. % TiB2 metal matrix composite. *Mater. Des.* 31: 3585–3589.

13. Padmanaban, G., and Balasubramanian, V. 2009. Selection of FSW tool pin profile, shoulder diameter and material for joining AZ31B magnesium alloy — An experimental approach. *Mater. Des.* 30: 2647–2656.

14. Gadakh, V. S., and Kumar, A. 2014. Friction stir welding window for AA6061-T6 aluminium alloy. *Proc IMechE, Part B: J Engineering Manufacture* 228(9):1172–1181.

15. Boz, M., and Kurt, A. 2004. The influence of stirrer geometry on bonding and mechanical properties in friction stir welding process. *Mater. Des.* 25: 343–347.

16. Suresha, C. N., Rajaprakash, B. M., and Upadhya, S. 2011. A study of the effect of tool pin profiles on tensile strength of welded joints produced using friction stir welding process. *Mater. Manuf.* 26(9): 1111–1116.

17. Ramanjaneyulu, K., Reddy, G. M., Rao, A. V., and Markandeya, R. 2013. Structure-property correlation of AA2014 friction stir welds: Role of tool pin profile. *J. Mater. Eng. Perform.* 22(8): 2224–2240.

18. Reddy, G. M., Sammaiah, P., Murthy, C. V. S., and Mohandas, T. 2002. Influence of welding techniques on microstructure and mechanical properties of AA 6061 (Al–Mg–Si) gas tungsten arc welds. *Proceedings of the Processing of Metals*, 33–46. PSG College of Technology, Coimbature, India.

19. Lohwasser, D., and Chen, Z. 2010. *Friction Stir Welding from Basics to Applications*. Woodhead Publishing Ltd.

20. Frigaard, Ø., Grong, Ø., Bjørneklett, B., and Midling, O. T. 1999. Modeling of the thermal and microstructural fields during friction stir welding of aluminium alloy. *First International Symposium on Friction Stir Welding*. Thousand Oaks, Calif.

21. Frigaard, Ø., Grong, Ø., and Midling, O. T. 2001. A process model for friction stir welding of age hardening aluminium alloys. *Metall. Mater. Trans. A.* 32: 1189–1200.

22. Hamilton, C., Dymek, S., and Sommers, A. 2008. A thermal model of friction stir welding in aluminium alloys. *Int. J. Mach. Tools. Manuf.* 48: 1120–1130.

23. Prasad, Y. V. R. K., and Sasidhara, S. 1997. *Hot Working Guide: A Compendium of Processing Maps*. ASM International.

24. Backer, J. D., Bolmsjö, G., and Christiansson, A.-K. 2014. Temperature control of robotic friction stir welding using the thermoelectric effect. *Int. J. Adv. Manuf. Technol.* 70: 375–383.

25. Zhang, X. X., Xiao, B. L., and Ma, Z. Y. 2011. A transient thermal model for friction stir weld. Part II: Effects of weld conditions. *Metall. Mater. Trans. A.* 42A: 3229–3239.

26. Elangovan, K., Balasubramanian, V., and Valliappan, M. 2009. Effect of welding speed and tool pin profile on tensile properties of friction stir welded AA6061 aluminium alloy. *Int. J. Microstructure and Materials Properties* 4(4): 455–475.